machines

Article

A Reference Governor with Adaptive Performance for Quadrotors under Safety Constraints

Panagiotis S. Trakas , Andreas Tantoulas and Charalampos P. Bechlioulis *

Department of Electrical and Computer Engineering, University of Patras, 26504 Patras, Greece; ptrakas@upatras.gr (P.S.T.); up1066582@upnet.gr (A.T.)
* Correspondence: chmpechl@upatras.gr

Abstract: This paper presents a novel robust reference governor (RG) for trajectory tracking of quadrotors. The proposed scheme is characterized by low computational complexity and straightforward gain selection. Moreover, it considers safety constraints regarding speed limits and ensures the stability and the proper operation of the closed-loop system. The proposed scheme imposes user-specified performance attributes on the evolution of the tracking error when the safety constraints allow it. When these constraints are at risk of violation, the proposed RG provides a relaxation of the predefined performance specifications to ensure the stability of the plant. Lyapunov analysis proves the boundedness of the closed-loop signals, while its efficacy is further clarified and verified via extensive comparative experimental results against a well-established PI regulator.

Keywords: adaptive performance control; input constraints; reference governor

Citation: Trakas, P.S.; Tantoulas, A.; Bechlioulis, C.P. A Reference Governor with Adaptive Performance for Quadrotors under Safety Constraints. *Machines* **2023**, *11*, 984. https://doi.org/10.3390/machines11110984

Academic Editors: Zafer Bingul and Ferat Sahin

Received: 22 September 2023
Revised: 20 October 2023
Accepted: 22 October 2023
Published: 24 October 2023

1. Introduction

1.1. Motivation

In recent years, there has been a notable surge of interest within the robotics and control communities in the realm of autonomous quadrotor systems. These agile unmanned aerial vehicles (UAVs), known for their mechanical simplicity, high maneuverability and the ability to perform vertical take-off and landing, have found versatile applications in areas such as payload transportation [1], search and rescue operations [2], forest fire monitoring [3], building inspections [4] and border surveillance [5].

Quadrotors are inherently nonlinear and unstable systems, possessing six degrees of freedom (DOFs) and only four control inputs, rendering them underactuated. Ensuring the safe and efficient operation of quadcopters is a critical requirement for executing tasks in real-world scenarios. The latter becomes more challenging when the designer considers complex dynamic models involving limitations of the actuators and safety constraints regarding the cruise speed. Moreover, achieving precise and safe maneuvering of a quadrotor is a formidable task when relying on manual control, which demands the execution of complex control inputs to maintain the desired cruising speed along a predefined trajectory, even in the absence of external disturbances. Consequently, *the development of effective and safe control strategies, capable of overcoming the limitations of manual operation and ensuring the quadrotor's precise and secure navigation, is of paramount importance.*

1.2. Related Literature

Typically, the majority of commercial drones are equipped with conventional linear control units, like PID and LQR schemes, owing to their low computational complexity, which is essential for realistic applications, where the decisions made by the plant have to be instantaneous. These controllers are suitable for shaping the dynamics locally, assuming that the quadcopter operates close to hovering conditions. However, in pursuit of enhancing flight conditions and performance across a wider range of scenarios, nonlinear control methods have also been developed by researchers over the years to tackle the challenges posed by the nonlinear nature of quadrotors [6]. These include feedback linearization methods [7–9] for transforming nonlinear dynamics into equivalent linear forms, backstepping controllers [10], sliding mode controllers [11] for robust stabilization and parameter adaptive laws [12]. Additionally, intelligent control approaches like fuzzy logic [13] and artificial neural networks [14] have been proposed to alleviate the need for precise knowledge of the dynamic model, though they often require substantial computational resources and trial-and-error parameter tuning, which renders these approaches impractical for online implementation. Finally, to counteract external time-varying disturbances affecting quadrotors, disturbance observer-based tracking controllers have been proposed (e.g., [15]).

As in most physical systems, quadrotors undergo severe actuation limitations. In particular, the motors of the plant can move up to a maximum speed and thus the thrust generated by the propellers of the system is bounded within a compact set. As a result, reference trajectories that require control commands outside of this set put the actuator at saturation conditions, since no further control effort can be applied to the system. The saturation effect constitutes one of the most harsh input nonlinearities as it can lead the system to instability. A few methods that address input constraints for quadrotor control include optimization-based approaches [16,17]. The practical limitation of these techniques, though, arises from their computational burden. Low-complexity control schemes include Lyapunov-based methodologies [18–20]. Funnel-based approaches [21–23] have also been studied for the quadcopter's tracking-control problem in [24,25]. However, when the tracking-error approaches the constraint boundary the excessive control inputs can potentially exceed input limits and lead to system instability. In [26], the authors introduced an observer-based adaptive fuzzy attitude control approach that achieves finite-time convergence while addressing input constraints. This scheme demonstrates exceptional robustness in the face of system uncertainties and actuation constraints, making it a valuable contribution. Furthermore, it contributes to reducing the computational complexity typically associated with fuzzy control methods. In [27], a method was introduced for adaptive robust fault-tolerant control in spacecraft proximity operations. Additionally, the tracking-control problem for small fixed-wing UAVs with input and state constraints was addressed in [28] through a robust approximation-free control strategy. A novel control approach considering output performance specifications while simultaneously addressing magnitude and rate constraints with respect to the input control signal was recently proposed in [29]. This controller was used to efficiently prevent the wing-rock phenomenon for a delta wing UAV. An alternative method dealing with input constraints is reference governors (RGs) [30,31]. The key concept of RGs is the separation of the controller design from the task of ensuring constraint satisfaction. More specifically, by assuming the presence of a predesigned controller capable of stabilizing the system and ensuring effective tracking in unconstrained scenarios, the RG is a nonlinear component integrated into the plant in order to enforce constraints. That involves adjusting the reference signals fed to the stabilizing control unit whenever it is necessary to ensure constraint satisfaction. Nevertheless, the majority of RG approaches rely on online optimization methods; i.e., the computation time and complexity increase with the number of constraints [32]. The issue of computational complexity in RGs was addressed in [33], where the authors map the constraints into an upper bound of a Lyapunov function regulating the applied reference signal to enforce this boundary.

1.3. Contributions

In this work, motivated by the aforementioned discussion, we propose a novel robust RG for quadrotors with safety input constraints. In particular, we build on our previous work on adaptive prescribed performance control (APPC) [34] to design an approximation-free control scheme aiming at modifying the reference trajectory, regarding the translational and yaw motion of the plant, to meet preassigned safety constraints. By safety constraints, we mean a set of reference speeds within which the quadrotor moves safely, away from saturation and aerobatic flight effects. In other words, safety sets correspond to reference trajectories for which the onboard controllers can effectively stabilize the system. The main contributions of this work are listed as follows:

1. In contrast to the majority of the related literature [16,17,26,30,31], the proposed control scheme is approximation-free and is characterized by low computational complexity.
2. Compared to [26], the values of control gains have a minor effect on the control performance and the tuning procedure is simple.
3. The proposed scheme exhibits robustness on actuation and feedback faults that cause control signal chattering.
4. Contrary to [33], the proposed RG imposes performance specifications on the output tracking error in accordance with the safety constraints.

2. Problem Formulation and Preliminaries

Let us first define the inertial frame $\mathcal{I} := \{e_x^I, e_y^I, e_z^I\}$, which is located at a fixed position on the ground and oriented in the north-west-up (NWU) convention as depicted in Figure 1.

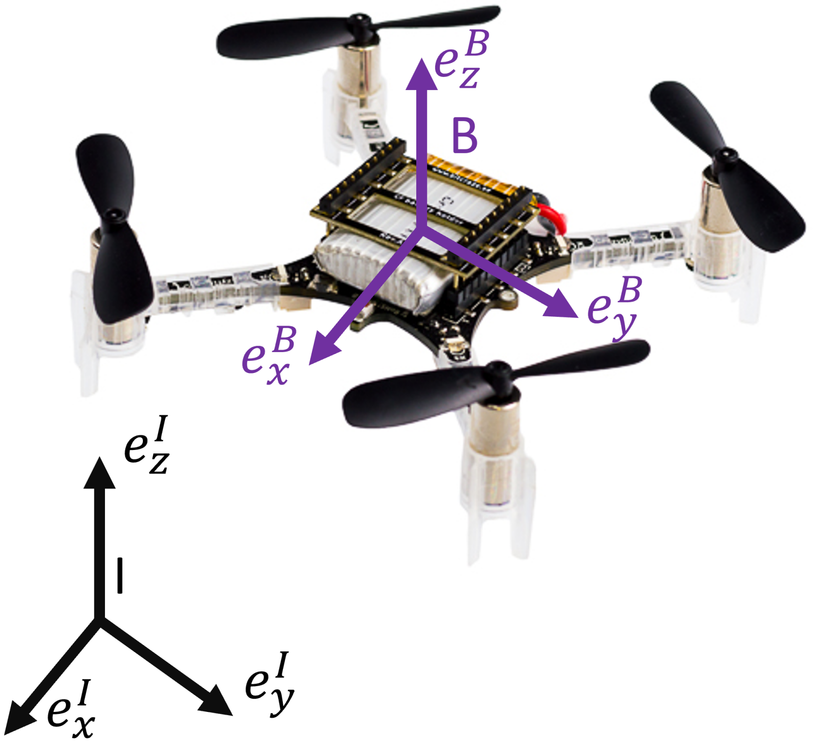

Figure 1. The Crazyflie 2.1 nano-quadcopter. The inertial frame $\mathcal{I}$ is depicted with black color and the body-fixed frame $\mathcal{B}$ with purple.

Furthermore, the body frame is attached at the center of gravity of the drone and it is denoted $\mathcal{B} := \{e_x^B, e_y^B, e_z^B\}$. A quadrotor can be modeled as an underactuated six-DOF nonaffine dynamical system as follows:

$$
\begin{aligned}
\dot{v} &= -g\begin{bmatrix}0\\0\\1\end{bmatrix} + \boldsymbol{R}(\boldsymbol{\phi})\frac{T}{m} \\
\dot{w} &= I^{-1}\left(\begin{bmatrix}(I_{yy}-I_{zz})qr\\(I_{zz}-I_{xx})\chi r\\(I_{xx}-I_{yy})\chi q\end{bmatrix} + \tau\right)
\end{aligned}
\tag{1}
$$

where $v = [\dot{x}, \dot{y}, \dot{z}]^T \in \mathbb{R}^3$, $w = [\chi, q, r] \in \mathbb{R}^3$ denote the linear and angular velocity of the system, expressed in $\mathcal{I}$. Additionally, g is the gravitational acceleration, $\boldsymbol{R}(\boldsymbol{\phi})$ is a rotation matrix that maps $\mathcal{B}$ into $\mathcal{I}$, m denotes the mass of the quadrotor and $I = \text{diag}(I_{xx}, I_{yy}, I_{zz})$ with I_{xx}, I_{yy}, I_{zz} denoting the moments of inertia with respect to the principal axes of $\mathcal{B}$. The net thrust generated by the propellers of the vehicle is denoted T and $\tau = [\tau_\phi, \tau_\theta, \tau_\psi]^T \in \mathbb{R}^3$ contains the rolling, pitching and yawing moments, respectively. Finally, the Euler rate vector $\dot{\boldsymbol{\phi}} = [\dot{\phi}, \dot{\theta}, \dot{\psi}]^T$ and the angular velocity w, expressed in $\mathcal{I}$, are related via the following equation:

$$\dot{\boldsymbol{\phi}} = E(\boldsymbol{\phi})w.$$

A detailed presentation of $\boldsymbol{R}(\boldsymbol{\phi}), E(\boldsymbol{\phi}), I, T$ and τ can be found in [35].

2.1. Control Objective

Cascade PID control schemes are frequently utilized to achieve quadrotor stabilization in realistic scenarios, owing to their inherent nonlinear attributes [36]. Such controllers typically involve an outer loop for stabilizing the position of the plant and a second, faster inner attitude controller responsible for stabilizing the quadcopter's orientation. The aforementioned stabilizing control unit is typically implemented onboard the system as it relies on feedback from an onboard inertial measurement unit (IMU) that enables rapid control command updates. As quadrotors are underactuated systems, we can only control four out of six DOFs at a time. In this work, we aim at enforcing the quadrotor to track a desired translational motion with specific yaw angle; i.e., the output of the system is $o(t) = [x(t), y(t), z(t), \psi(t)]^T$. Note that given a fast time-varying reference signal or a sudden wind gust, the onboard controller will generate large control signals ω that may degrade the overall performance of the system, giving rise to undesired actuation saturation or high velocities that put the plant at risk. In order to address the aforementioned problem, it is essential that the reference trajectory $o_d(t) = [x_d(t), y_d(t), z_d(t), \psi_d(t)]^T$ is incorporated into a control signal $u(t)$ that remains constrained within a safety set $\mathcal{U}$ away from high speeds and saturation effects, i.e., $u(t) \in \mathcal{U}$ with $\mathcal{U} := \{u \in \mathbb{R}^4 : |u_i(t)| \leq \bar{u}_i,\ i = 1, \ldots, 4\}$ for some properly chosen upper bounds $\bar{u}_i > 0$. Note that the vector u contains the velocity-control commands regarding the translational and yaw motion of the system considering safety constraints and it is fed to the internal controller that regulates properly the velocities of each motor to achieve the desired response of the quadcopter. In this vein, the objective of this work lies in proposing a low-complexity reference governor, i.e., a control command $u(t) \in \mathcal{U}$, with adaptive transient and steady-state performance specifications that regulates the reference signal and guarantees:

- Adaptive performance characteristics on the output tracking error $e(t) = o(t) - o_d(t)$ of the closed-loop system.
- The safe operation of the quadrotor, considering velocity constraints.
- The boundedness of all signals in the closed-loop system.

Let us now define the position vector $p = [x,\ y,\ z]^T$ and the reference position vector $p_d(t) = [x_d(t),\ y_d(t),\ z_d(t)]^T$ and pose the following necessary assumptions:

Assumption 1. *The onboard controllers of the quadrotor are able to stabilize the states of the system within a known compact safety set $\mathcal{U}$.*

Assumption 2. *The dynamics of (1) is described by continuous, with respect to the states of the system, functions.*

Assumption 3. *The reference trajectory $o_d(t) = [p_d^T(t), \psi_d(t)] \in \mathbb{R}^4$ and its first derivative $\dot{o}_d(t)$ are known functions of time.*

Remark 1. *Assumption 1 plays a crucial role in the design of a Reference Generator (RG), as it ensures the system's stability by relying on the internal control unit of the plant. In this study, we make the assumption that the onboard controllers of the quadrotor are capable of maintaining* *stability within a defined set $\mathcal{U}$, which includes "safe" reference velocity signals. Assumption 2 ensures the avoidance of impulsive behaviour regarding the states of the system, which can lead to PPC singularity; i.e., it forces the tracking error to exceed the performance envelope, resulting in unbounded control signals. Finally, Assumption 3 pertains to the availability of knowledge about the reference trajectory and its first derivative that serves as a feedforward term (refer to Section 3) enhancing the closed-loop performance. Omitting reference velocity information is possible without affecting the boundedness of the signals in the control loop, although it may result in larger control inputs.*

2.2. Preliminaries on Adaptive Performance Control

Adaptive performance [34] concerns the evolution of the output tracking error strictly within a time-varying set that encapsulates the desired transient and steady-state performance requirements. In particular, consider a tracking error $e(t)$ available for measurement. Adaptive performance is accomplished if $e(t)$ evolves strictly within an envelope defined by functions $\rho(t), -\rho(t)$, with $\rho : \mathbb{R}_+ \to \mathbb{R}_+^*$ called Performance Function (PF) and properly designed to encapsulate the performance attributes and adjust according to the input constraints. By appropriately designing an adaptive law for the differentiable performance function $\rho(t)$, performance specifications on the evolution of the tracking error $e(t)$ are imposed with respect to the transient period and the absolute steady-state error, while also considering their conflict with the actuator's constraints. Note that since the actuator becomes saturated, the performance envelope has to be adjusted in order to enclose the tracking error and ensure the adaptive performance and the boundedness of closed-loop signals. On the other hand, when the actuator operates away from saturation the performance envelope restores its prescribed form exponentially quickly.

3. Controller Design

In this section, we first propose a reference governor with adaptive performance considering safety constraints and then we prove that all closed-loop signals remain bounded. The control design consists of two steps. First, we design the position controller and subsequently we exploit the estimate of the yaw angle in order to design the orientation control law.

Step 1. Given a desired translational trajectory $p_d(t)$, we define the output tracking error $e_p(t) = p(t) - p_d(t) \in \mathbb{R}^3$. Next, let us define the matrix $R(t) = \text{diag}(\rho_1(t), \rho_2(t), \rho_3(t)) \in \mathbb{R}^{3\times3}$ with $\rho_i(t),\ i = 1, 2, 3$ denoting the adaptive performance function of the i-th output. Hence, the normalized position error is given as $\xi(t) = R^{-1}(t)e_p(t) \in \prod_{i=1}^{3}(-1, 1)$ for $|e_{p_i}| < \rho_i$. Exploiting the APPC technique, we select the diffeomorphism $\text{atanh} : (-1, 1) \to (-\infty, \infty)$ in order to map $\xi(t)$ onto R^3. Thus, the transformed error is denoted as $\epsilon(t) = [\text{atanh}(\xi_1(t)), \text{atanh}(\xi_2(t)), \text{atanh}(\xi_3(t))]^T$. The proposed control law concerning the translational motion of the quadrotor is given as follows:

$$v_d(t) = -K\mathcal{D}(t)\left(\epsilon + A\int_0^t \epsilon(\tau)d\tau\right) + \dot{p}_d(t) \tag{2}$$

where $\mathcal{D}(t) = \text{diag}(d_1(t), d_2(t), d_3(t))$ with $d_i(t) = \frac{1}{(1-\xi_i^2(t))\rho_i(t)}$ denoting a positive gain that increases as $|\xi_i(t)| \to 1$, scaling the control signal when the tracking-error approaches the performance envelope. Furthermore, the diagonal matrices $K = \text{diag}(k_1, k_2, k_3)$ $A = \text{diag}(a_1, a_2, a_3)$ with $k_i, a_i > 0$ are constant gain matrices and $\dot{p}_d(t)$ is the derivative of the reference trajectory $p_d(t)$, i.e., the reference velocity. The input constraints are incorporated via a saturation function. In this work, we adopt a typical symmetrical saturation function; thus, the constrained control signal is given by:

$$v_i(t) = \text{sat}(v_{d_i}(t)) = \begin{cases} \bar{u}_i & \text{if} \quad v_{d_i} > \bar{u}_i \\ v_{d_i} & \text{if} \ |v_{d_i}| \leq \bar{u}_i \\ -\bar{u}_i & \text{if} \quad v_{d_i} < -\bar{u}_i \end{cases} \tag{3}$$

for all $i = 1, 2, 3$, with $\bar{u}_i$ denoting the maximum absolute value of a velocity to be considered safe. The position controller is then augmented via an adaptive law that adjusts the performance boundaries according to the saturation condition of the control signal. In particular, the adaptive performance envelope is obtained by:

$$\dot{\rho} = -\Lambda(\rho(t) - \rho^\infty) + \Xi^{-1}(v(t) - v_d(t)) \tag{4}$$

where $\Lambda = \text{diag}(\lambda_1, \lambda_2, \lambda_3)$, $\Xi(t) = \text{diag}(\xi_1(t), \xi_2(t), \xi_3(t))$, $v(t) = [v_1(t), v_2(t), v_3(t)]^T$, $\rho(t) = [\rho_1(t), \rho_2(t), \rho_3(t)]^T$, $\rho^\infty = [\rho_1^\infty, \rho_2^\infty, \rho_3^\infty]^T$ with $\rho_i(0) > |e_{p_i}(0)|$ to ensure that $\xi(0) \in \prod_{i=1}^{3}(-1, 1)$ and the positive control performance parameters λ_i, ρ_i^∞ are properly selected. More specifically, ρ_i^∞ represents the maximum allowable absolute value of the tracking error in steady state and the choice of constant λ introduces a lower limit on the speed at which $e(t)$ converges to the steady state. Notice that the first term in (4) corresponds to the decaying PF that incorporates the user-specified performance attributes, while the second term is activated when the reference velocity reaches the safety bounds in order to relax the performance constraints. Such a compromise is necessary for the boundedness of the closed-loop signals, since when the tracking errors approach the performance boundary, i.e., $\xi_i(t) \geq 1$, then the transformed error $\epsilon_i(t)$ becomes unbounded and there is no guarantee that the tracking error will retain its prescribed attributes, putting the system at risk.

Step 2. Following the same reasoning as in Step 1 and given a desired yaw trajectory $\psi_d(t) \in \mathbb{R}$, we first define the yaw tracking error $e_\psi(t) = \psi(t) - \psi_d(t)$. Then, the transformed error $\epsilon_\psi(t) = \text{atanh}(\xi_\psi(t)) \in \mathbb{R}$ can be obtained by letting $\xi_\psi(t) = \frac{e_\psi(t)}{\rho_\psi(t)}$, for an adaptive PF $\rho_\psi(t)$. Hence, the yaw angle governor is given by:

$$\begin{aligned} v_{\psi_d}(t) &= -\frac{\epsilon_\psi(t)}{(1 - \xi_\psi^2)\rho_\psi(t)} + \dot{\psi}_d(t) \\ v_\psi(t) &= \text{sat}(v_{\psi_d}(t)) \\ \dot{\rho}_\psi &= -\lambda_i(\rho_\psi(t) - \rho_\psi^\infty) + \frac{v_\psi(t) - v_{\psi_d}(t)}{\xi_\psi(t)} \end{aligned} \tag{5}$$

with the performance parameters $\lambda_\psi, \rho_\psi^\infty$ selected to incorporate the desired convergence rate and absolute steady-state error boundaries, respectively, and $\rho_\psi(0) > |e_\psi(0)|$.

Consequently, the overall control signal u that is fed to the onboard controller of the quadrotor and guarantees operation of the system that is safe and away from saturation is given by $u(t) = [v_1(t), v_2(t), v_3(t), v_\psi(t)]^T \in \mathcal{U}$. For the reader's convenience, the closed-loop system is depicted in Figure 2 and the proposed RG is visualised in Figure 3.

Remark 2. *Note that the proposed control scheme neither leverages any knowledge about the system nonlinearities nor utilizes any approximation mechanism such as neural nets. Both the control signals and the adaptive performance laws are generated via simple calculations avoiding the explosion of complexity for the proposed control algorithm. Furthermore, the gain tuning is quite simple as it is shown in the stability analysis (the control gains do not affect the closed-loop performance significantly). Thus, the low complexity in combination with the easy tuning facilitate practitioners in implementing the proposed control approach and utilizing it in real tasks.*

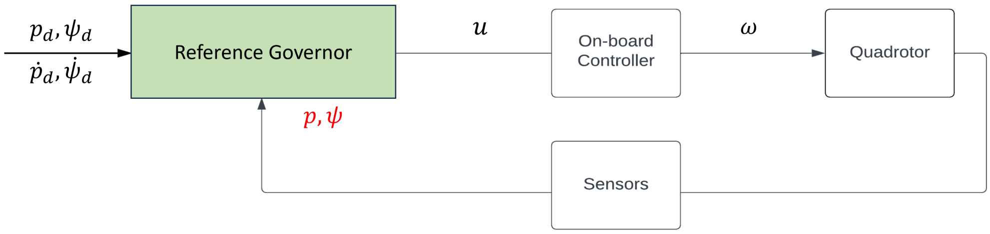

Figure 2. The proposed closed-loop control scheme.

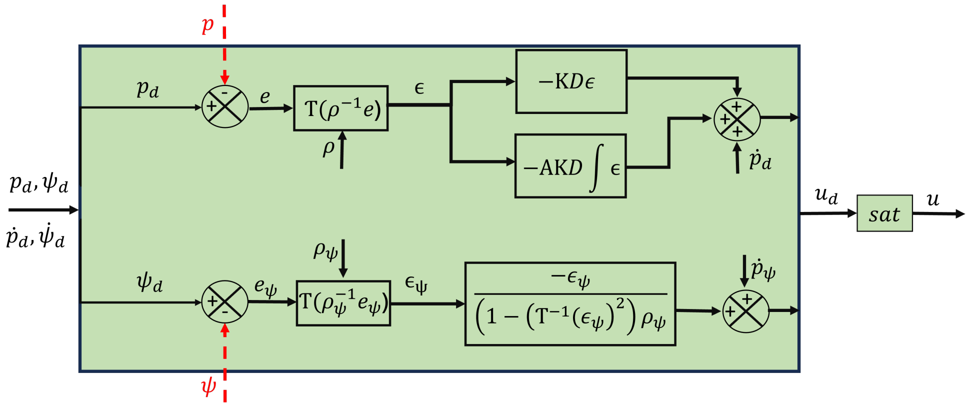

Figure 3. The proposed Reference Governor.

Theorem 1. *Consider a quadrotor satisfying Assumptions 1 and 2 and a reference trajectory $o_d(t)$ that satisfies Assumption 3. The proposed RG (2)–(5) ensures the stability of the closed-loop system for all $t \geq 0$ and imposes adaptive performance evolution of the tracking error $e(t) = o(t) - o_d(t)$, i.e., $\|e_i(t)\| \leq \rho_i(t)$, $i \in \{1,\ 2,\ 3,\ \psi\}$.*

Proof. Let us first introduce the dynamics of the augmented closed-loop dynamical system as:

$$\dot{\zeta} := h(\zeta, t) = [\dot{\xi}^T, \dot{\xi}_\psi, \dot{\rho}^T]^T. \tag{6}$$

Subsequently, we define the open set:

$$\Omega := \prod_{i=1}^{4}[(-1,1)] \times (0, \bar{\rho}_1) \times (0, \bar{\rho}_2) \times (0, \bar{\rho}_3) \times (0, \bar{\rho}_\psi) \subset \mathbb{R}^8$$

with $\bar{\rho}_i,\ i = 1,2,3,\psi$ denoting the upper bound of the i-th PF. Thenceforward, the proof includes two distinct phases. Firstly, we establish the existence of a unique maximal solution, denoted as $\zeta : [0, \tau_{\max}) \to \Omega$, for system (6). This entails that $\zeta(t)$ stays within the set Ω for all time instances t within the interval $[0, \tau_{\max})$. Subsequently, we provide a proof that demonstrates the continuous evolution of ζ within a compact subset of Ω. This particular insight has significant implications as it leads to a contradiction, eventually establishing that $\tau_{\max}$ extends to infinity.

Phase A. Consider the closed-loop dynamical system described by Equation (6). By design, we have the initial conditions such that $|\xi_i(0)| < 1$, $\rho_i(0) \in (0, \bar{\rho}i)$ for $i = 1,2,3,\psi$, ensuring that $\zeta(0) \in \Omega$. Additionally, we note that $\dot{\zeta}$ is piece-wise continuous and locally integrable with respect to time t and locally Lipschitz with respect to ζ over the open set Ω. Therefore, by exploiting Theorem 54 in [37] (p. 476) we establish the existence of a unique maximal solution $\zeta : [0, \tau_{\max}) \to \Omega$, which is valid for all instances within the interval $[0, \tau_{\max})$.

Phase B. In *Phase A* of our proof, we demonstrated that $\zeta(t) \in \Omega$ holds true for all instances within the interval $[0, \tau_{\max})$. The aforementioned implies that the transformed errors, denoted as ϵ_i, are well defined and bounded for every $t \in [0, \tau_{\max})$. This is because $\xi_i(t) \in (-1, 1)$ for all $i = 1, 2, 3, \psi$. We first elaborate on the boundedness of the translational motion signals. In this vein, consider the Lyapunov function candidate $L_1 = \frac{1}{2} r^T K r + \frac{1}{2} s^T A^2 K s$ with $s = [\int_0^t \epsilon_1(\tau)dt, \int_0^t \epsilon_2(\tau)dt, \int_0^t \epsilon_3(\tau)dt]^T$ and $r = \epsilon + As$. By time differentiating L_1 we obtain:

$$\begin{aligned}\dot{L}_1 &= r^T K \dot{\epsilon} + (\epsilon + As)^T AK\epsilon + s^T A^2 K\epsilon \\ &= r^T K\dot{\epsilon} + \epsilon^T AK\epsilon + 2s^T A^2 K\epsilon.\end{aligned}$$

Let us define the Jacobian of the error transformation vector as $J(\xi) = \mathrm{diag}(J(\xi_1), J(\xi_2), J(\xi_3))$ with $J(\xi_i) = \frac{1}{1-\xi_i^2}$, which entails $\dot{\epsilon} = J(\xi)\dot{\xi}$. Exploiting the latter, adding and subtracting $s^T A^3 s$ and substituting (2), (4) into $\dot{L}_1$, we arrive at:

$$\dot{L}_1 = r^T KJ(\xi(t))R^{-1}(t)\Big(\dot{p} + E_p(t)\Lambda(1 - R^{-1}(t)\rho^\infty) - \boldsymbol{v} - KJ(\xi(t))R^{-1}(t)r\Big) + r^T AKr - s^T A^3 s. \tag{7}$$

where $E_p(t) = \mathrm{diag}(e_{p_1}(t), e_{p_2}(t), e_{p_3}(t))$ and $r^T AKr = \epsilon^T AK\epsilon + \epsilon^T A^2 Ks + s^T A^2 K\epsilon + s^T A^3 Ks$. Next, owing to the boundedness of the reference input $\boldsymbol{v}$, the fact that $\xi_i(t) \in (-1, 1), \rho_i(t) \in (0, \bar{\rho}i)$ for $i = 1, 2, 3$ and invoking Assumptions 1 and 2, we obtain:

$$\bar{b} := \max_{\zeta \in \Omega}\Big\{\Big\|KJ(\Xi(t))R^{-1}(t)\Big(\dot{p} + E_p(t)\Lambda(1 - R^{-1}(t)\rho^\infty) - \boldsymbol{v}\Big)\Big\|\Big\}.$$

Additionally, $\frac{J(\xi_i(t))}{\rho_i(t)} = \frac{\rho_i(t)}{(\rho_i^2 - e_{p_i}^2(t))} > \frac{|\xi_i(t)|}{(1-\xi_i^2(t))e^*_{p_i}}$ with $e^*_{p_i}$ denoting the upper bound of the tracking error owing to Assumption 1. Since $\frac{J(\xi_i(t))}{\rho_i(t)}$ is increasing on $\xi_i(t)$, there exists a vector ξ^* such that the square matrix $\Gamma = (KJ(\xi^*)R^{-1}(t))^2 - KA$ is positive definite; thus, $\dot{L}_1$ satisfies:

$$\dot{L}_1 \leq \bar{b}\|r\| - \|\Gamma r\|^2 - a_{\min}\|s\|^2 \tag{8}$$

where $a_{\min}$ denotes the smallest value of the diagonal matrix A^3. Thus, $\dot{L}_1 < 0$ when $r_i(t) > \bar{r}_i$, $i = 1, 2, 3$ for the positive constants $\bar{r}_i = \frac{\bar{b}}{k_i(k_i(\xi_i^*/e^*_{p_i})^2 - a_i)}$, leading to the ultimately uniform boundedness of $r(t)$ with respect to a compact set $\mathcal{R} := \prod_{i=1}^{3} \mathcal{R}_i$ with $\mathcal{R}_i := \Big\{r_i : |r_i(t)| \leq \max_{\zeta \in \Omega}\{|r_i(0)|, \bar{r}_i\}\Big\}$. Note that $\bar{r}_i$ does not depend on the upper bound of the adaptive PF $\bar{\rho}_i$ for all $i = 1, 2, 3$, because of the boundedness of the tracking error $e_{p_i}(t)$, by construction. Notice also that the second term of (4) is activated when $\xi_i(t) \geq \tilde{\bar{\xi}}$ for $\tilde{\bar{\xi}} > 0$ which depends on the size of $\mathcal{U}$. Moreover, the boundedness of $r_i(t)$ entails the boundedness of $\epsilon_i(t), \xi_i(t)$, i.e., $|\epsilon_i(t)| < \bar{\epsilon}_i$, $|\xi(t)| < \bar{\xi}_i$. Thus, there exists a performance bound $\bar{\rho}_i$ at a time instant $t = t_p$, such that the right hand side of (4) becomes negative when $\rho_i(t) = \bar{\rho}_i$. In particular, leveraging (4), we conclude that $\dot{\rho}_i < 0$ when:

$$\rho_i(t) > \frac{k_i J(\bar{\xi}_i)\bar{r}_i - \boldsymbol{v}_i}{\lambda_i \tilde{\bar{\xi}}_i} + \rho_\infty. \tag{9}$$

for all $i = 1, 2, 3$. The latter implies the existence of a small positive constant δ_i such that $\rho_i(t) \in [\rho_i^\infty, \bar{\rho}_i - \delta_i], \forall t \in [0, \tau_{\max})$.

Next, we condiser the yaw dynamics which is decoupled from the position. Hence, we select the *Lyapunov* function candidate $L_2 = \frac{1}{2}\epsilon_\psi^2$. By differantiating L_2 with respect to time and manipulating as in the previous step, we can easily arrive at:

$$\dot{L}_2 \leq \left|\frac{J(\xi_\psi(t))\epsilon_\psi(t)}{\rho_\psi(t)}\right|\bar{c} - \left|\frac{J(\xi_\psi(t))\epsilon_\psi(t)}{\rho_\psi(t)}\right|^2. \tag{10}$$

where:

$$\bar{c} := \max_{\zeta\in\Omega}\left\{\left\|\left(\dot{\psi} + (\psi(t) - \psi_d(t)\lambda_\psi\left(1 - \frac{\rho_\psi^\infty}{\rho_\psi(t)}\right) - v_\psi(t)\right)\right\|\right\}$$

which applies because of the boundedness of $v_\psi(t)$ and exploiting Assumptions 1 and 2. Thus, $\dot{L}_2 < 0$ for $|\epsilon_\psi(t)| > \frac{\bar{c}\bar{e}_\psi}{\xi_\psi^*}$ with ξ_ψ^* denoting the smallest value of $\xi_\psi(t)$ for which the relaxation of the performance envelope of yaw tracking error is activated and $\bar{e}_\psi = \max\{|\psi(t) - \psi_d(t)|\}$. The latter implies that $|\epsilon_\psi(t)| \leq \bar{\epsilon}_\psi = \max\left\{\epsilon_\psi(0), \frac{\bar{c}\bar{e}_\psi}{\xi_\psi^*}\right\}$. Finally, since $\bar{\epsilon}_\psi$ does not depend on the magnitude of the adaptive PF $\rho_\psi(t)$ there exists a $\bar{\rho}_\psi > 0$ such that $\dot{\rho}_\psi < 0$ when $\rho_\psi(t) > \bar{\rho}_\psi$, ensuring the existence of a positive constant δ_ψ such that $\rho_\psi(t) \in [\rho_\psi^\infty, \bar{\rho}_\psi - \delta_\psi], \forall t \in [0, \tau_{\max})$.

Hence, we have established the boundedness of the transformed error $\epsilon_i(t) = \operatorname{atanh}(\xi_i(t))$ within a compact subset of $\mathbb{R}$, entailing the boundedness of normalized errors $\xi_i(t)$ within $\Omega_{\xi_i} = [\underline{\xi}_i, \overline{\xi}_i] \subset (-1, 1)$ and adaptive performance functions $\rho_i(t)$ within $\Omega_{\rho_i} \subset (0, \bar{\rho}_i)$ $\forall t \in [0, \tau_{\max})$ for all $i = 1, 2, 3, \psi$. Notably, the augmented system's solution, i.e., $\zeta(t)$, consistently resides in the set Ω', with $\Omega' := \Omega_{\xi_i} \times \Omega_{\rho_i}$, $i = 1, 2, 3, \psi$. Assuming a finite $\tau_{\max}$, Proposition C.3.6 in [37] leads to a contradiction, asserting the existence of a time instant τ' where $\zeta(\tau')$ exits Ω'. Consequently, we deduce that $\tau_{\max}$ must be infinite, affirming the boundedness of closed-loop signals. Finally, exploiting the fact that $\xi_i(t) \in \Omega_{\xi_i}$, $i = 1, 2, 3, \psi$ for all $t \geq 0$ we conclude that:

$$|o_i(t) - o_{d_i}(t)| < \rho_i(t) < \bar{\rho}_i$$

for all $i = 1, 2, 3, \psi$ and $\forall t \geq 0$, which completes the proof. □

Remark 3. *The stability results of Theorem 1 are semi-global, owing to Assumption 1. According to that, the onboard controllers of the quadrotor are capable of stabilizing the system for a given set of reference signals that are strictly within the compact set $\mathcal{U}$. The size of $\mathcal{U}$ depends on the characteristics of the system, e.g., the load of the quadrotor, the maximum thrust that can be generated by the propellers as well as the feedback update speed. Thus, internal uncertainties and faults are encountered by the onboard control unit, while the proposed control RG enhances the robustness of the closed-loop system against external disturbances, e.g., wind gusts, by modifying the reference input. Specifically, by imposing constraints on the control input commands, the low-level internal controller can manage input perturbations more efficiently, allocating more resources to the stabilization of the plant.*

Remark 4. *Theoretical analysis has revealed semi-global stability characteristics for the closed-loop system that remain unaffected by the choice of control parameters, simplifying the process of parameter selection. Nonetheless, there are certain factors that need to be considered in the gain-tuning procedure. Firstly, the performance parameter ρ_i^∞, $i \in \{1, 2, 3, \psi\}$, corresponding to the maximum steady-state absolute error, should align with the precision of the sensors, as information below this level of accuracy cannot be reliably obtained from the plant. Furthermore, regarding the convergence rate parameters λ_i, $i \in \{1, 2, 3, \psi\}$, it is essential to take into account the initial tracking error $e_i(0)$. Opting for excessively large values of λ_i might result in significant control signal magnitude, potentially leading to saturation and, consequently, relaxing the achievable convergence rate specifications. Lastly, it is advisable to keep the control gains k_i, a_i, $i = 1, 2, 3$*

relatively small. This strategy helps prevent excessive amplification of the control signal, particularly in steady-state conditions, which could ultimately lead to saturation, i.e., performance degradation.

Remark 5. *While we initially assumed the quadrotor to be a symmetrical mechanical system, it is important to note that the results obtained in this study remain applicable even when dealing with mass asymmetry. Mass asymmetry is a common characteristic in real-world scenarios, especially in applications like parcel-delivery quadrotors. This assertion can be straightforwardly validated as the proposed control method does not rely on specific knowledge of the system dynamics. However, in cases of mass asymmetry, certain rotors of the UAV may need to spin faster to counterbalance the effects of uneven mass distribution. This, in turn, can lead to quicker rotor saturation, potentially affecting the safety compact set $\mathcal{U}$ within which the system's stability is assured by internal controllers. Therefore, further investigation in this direction is warranted to address and understand these implications. Additionally, there are other limitations in this work that need consideration. Those include the incorporation of acceleration constraints in addition to velocity constraints and the development of an identification mechanism capable of leveraging system knowledge. Such a mechanism would help prevent the controller from generating excessively large input signals that might result in unnecessary saturation activation.*

4. Experimental Results

In this section, we present the experimental results of the integration of the proposed RG on a commercial quadrotor, the Crazyflie 2.1 (https://www.bitcraze.io/products/crazyflie-2-1/, accessed on 17 September 2023), equipped with a cascade PID onboard control scheme that compensates for the inertial dynamics. In order to show the effectiveness and the superiority of our approach, we consider two different experimental scenarios and we compare the obtained results with a well established PI control unit utilized as RG. In particular, given the position-tracking error $e(t) = p(t) - p_d(t)$ the control signal fed by the PI RG to the onboard controllers of the drone is given as $u(t) = K_P e(t) + K_I \int_0^t e(\tau) d\tau + \dot{p}_d$ with $K_P = \mathrm{diag}(k_{px}, k_{py}, k_{pz})$, $K_I = \mathrm{diag}(k_{ix}, k_{iy}, k_{iz})$ for some gain matrices. A fine-tuning procedure was followed to select the gains of the PI RG. We decided to select the PI scheme as a benchmark owing to its simplicity and low computational complexity, which are comparable to the ones in our approach. All the experiments were conducted in our lab using the associated Loco Positioning system (https://www.bitcraze.io/documentation/system/positioning/loco-positioning-system/, accessed on 17 September 2023) to measure the position of the quadcopter with respect to its inertial frame $\mathcal{I}$. Additionally, since the estimates of the yaw angle appeared inaccurate because of the noisy sensing, we dropped the specification regarding the yaw angle tracking and we only consider the tracking problem of translational reference trajectories with fixed orientation. The performance parameters and the safety constraints for the proposed RG as well as the control gains for both schemes are presented in Table 1 and they are kept unaltered in all experimental studies.

Table 1. Control Scheme Parameters.

PPC Parameter	Value	PI Parameter	Value
$k_i,\ i = 1,2,3$	1	k_{px}	0.55
$a_i,\ i = 1,2,3$	1	k_{py}	0.55
$\lambda_i,\ i = 1,2,3$	0.5	k_{pz}	0.8
$\rho_i^\infty,\ i = 1,2,3$	0.15	k_{ix}	0.5
$\bar{u}_i\ i = 1,2$	0.45	k_{iy}	0.4
$\bar{u}_3$	0.25	k_{iz}	0.35

4.1. Circular Trajectory

In the first experimental study, we force the robot to move towards a desired position and then implement a circular trajectory twice. In particular, the reference trajectory is given by:

$$p_d(t) = \begin{cases} [0, 0, 0.6]^T, & 0 \leq t < T_1 \\ [-0.4, 0, 1.3]^T, & T_1 \leq t < T_2 \\ [0.4\cos(0.45(t - T_2) + \pi), 0.4\sin(0.45(t - T_2) + \pi), 1.3]^T, & t \geq T_2 \end{cases}$$

with $T_1 = \inf_{t>0}\{t \in \mathbb{R}_+ : e_p(t) \leq 0.1\}$ and $T_2 = \inf_{t>T_1}\{t \in \mathbb{R}_+ : e_p(t) \leq 0.1\}$. The output response of the plant along with the reference trajectory with respect to its principal axis is depicted in Figure 4, where the left subfigures illustrate the output performance of the proposed RG while the right ones depict the tracking performance of the PI regulator. The superiority of the proposed scheme is evident and it is also shown in Figure 5, where the evolution of the tracking errors is depicted, both for the proposed APC scheme (left) and the PI one (right). Note that the proposed RG maintaints the absolute tracking error less than 0.15 m at steady state while the corresponding tracking error under the PI scheme is significantly larger. Notice that the duration of motion of the quadrotor under the proposed scheme is greater than the one under the PI unit. The reason is the speed limits that are imposed by the proposed RG to prevent jerky movements and saturation nonlinearities until the drone reaches the first two fixed reference positions, i.e., $t = T_1$ and $t = T_2$. Finally, the control signals produced by each Reference Governor (RG) are displayed in Figure 6. It is apparent that the control effort with the proposed RG (on the left) is more intense than that of the PI controller. This increased control effort is a result of the imposition of output performance specifications by the proposed controller, which effectively regulates the control signal to ensure the tracking error converges nearly to zero at a predefined rate.

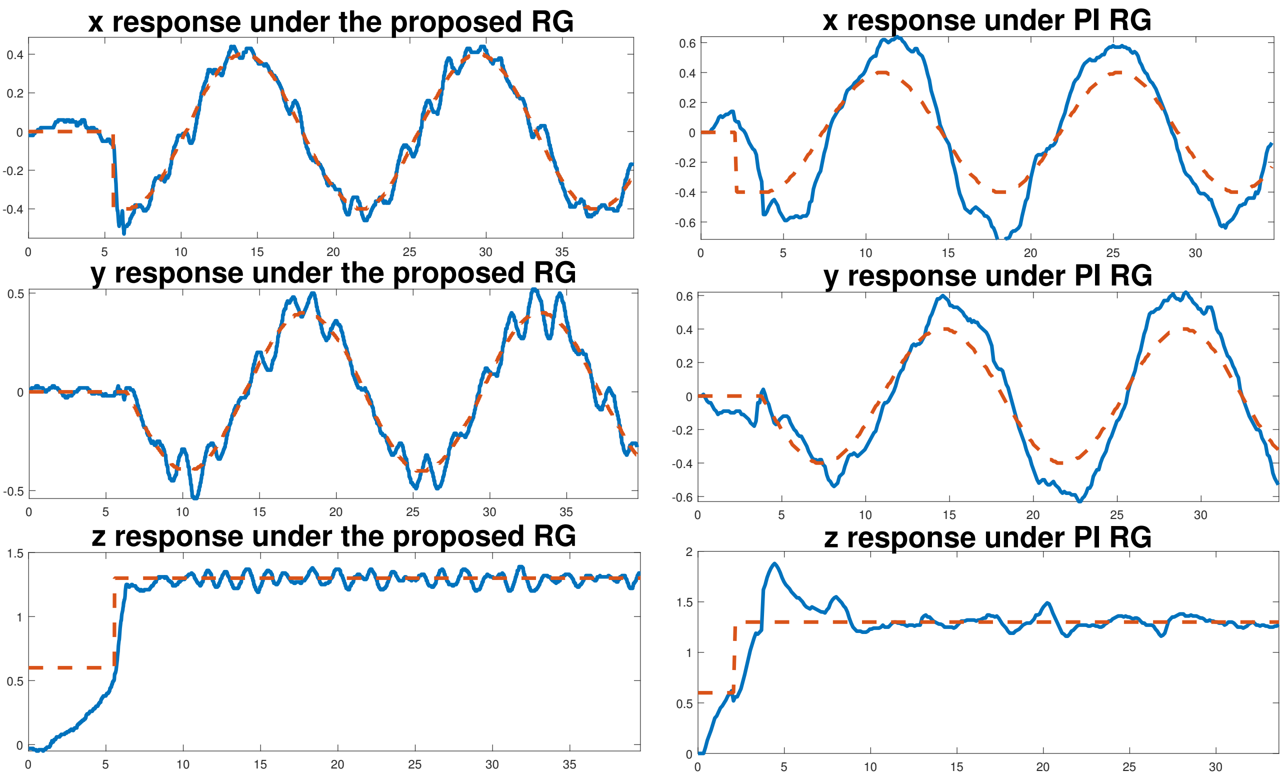

Figure 4. Circular trajectory: Time response of the quadrotor under the proposed (**left**) and PI (**right**) RGs. The orange dashed line corresponds to the reference trajectory with respect to its principal axis. The blue solid line corresponds to the actual response of the system.

4.2. Spiral Trajectory

In this experimental study, we set the robot to move again towards a fixed position and then track a spiral trajectory which is given by:

$$p_d(t) = \begin{cases} [0, 0, 0.6]^T, & 0 \leq t < T_1 \\ [-0.4, 0, 1.3]^T, & T_1 \leq t < T_2 \\ [-0.4\cos(0.45(t-T_2)), -0.4\sin(0.45(t-T_2)), 1.3 - 0.035(t-T_2)]^T, & t \geq T_2 \end{cases}$$

with $T_1 = \inf_{t>0}\{t \in \mathbb{R}_+ : e_p(t) \leq 0.1\}$ and $T_2 = \inf_{t>T_1}\{t \in \mathbb{R}_+ : e_p(t) \leq 0.1\}$.

As in the previous scenario, Figure 7 illustrates the system's response along with the reference trajectory. In the left subfigures, we showcase the output performance of the proposed RG, while the right subfigures depict the tracking performance of the PI regulator. The superiority of our scheme becomes evident, as further illustrated in Figure 8, which demonstrates the evolution of the tracking errors for the proposed scheme (left) and the PI controller (right). Notably, the absolute tracking error under the proposed controller remains again less than 0.15 meters at steady state, whereas the PI scheme fails to maintain similar tracking accuracy. Additionally, similar to the circular trajectory case, the enforcement of performance specifications results in a more intensive control effort under the proposed RG compared to the PI RG, as can be seen in Figure 9. Finally, Figure 10 provides a three-dimensional representation of the motion alongside the reference trajectory. The upper subfigures offer different perspectives of the motion under the proposed scheme, while the lower ones depict the motion under the PI governor.

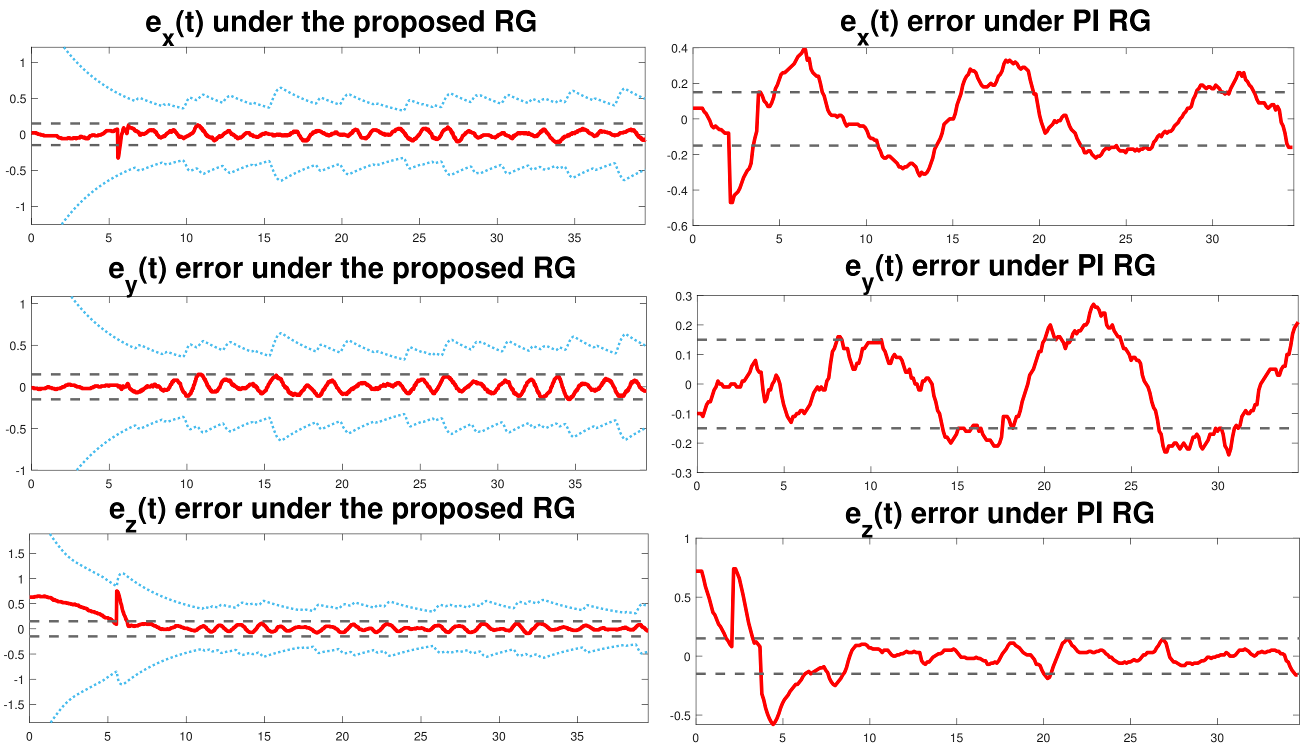

Figure 5. Circular Trajectory: Output tracking-error evolution of the quadrotor under the proposed (**left**) and PI (**right**) RGs. The light blue dotted lines correspond to the adaptive PFs. The grey dash-dotted lines correspond to the prescribed steady-state error bounds. The red solid line corresponds to the tracking error with respect to its principal axis.

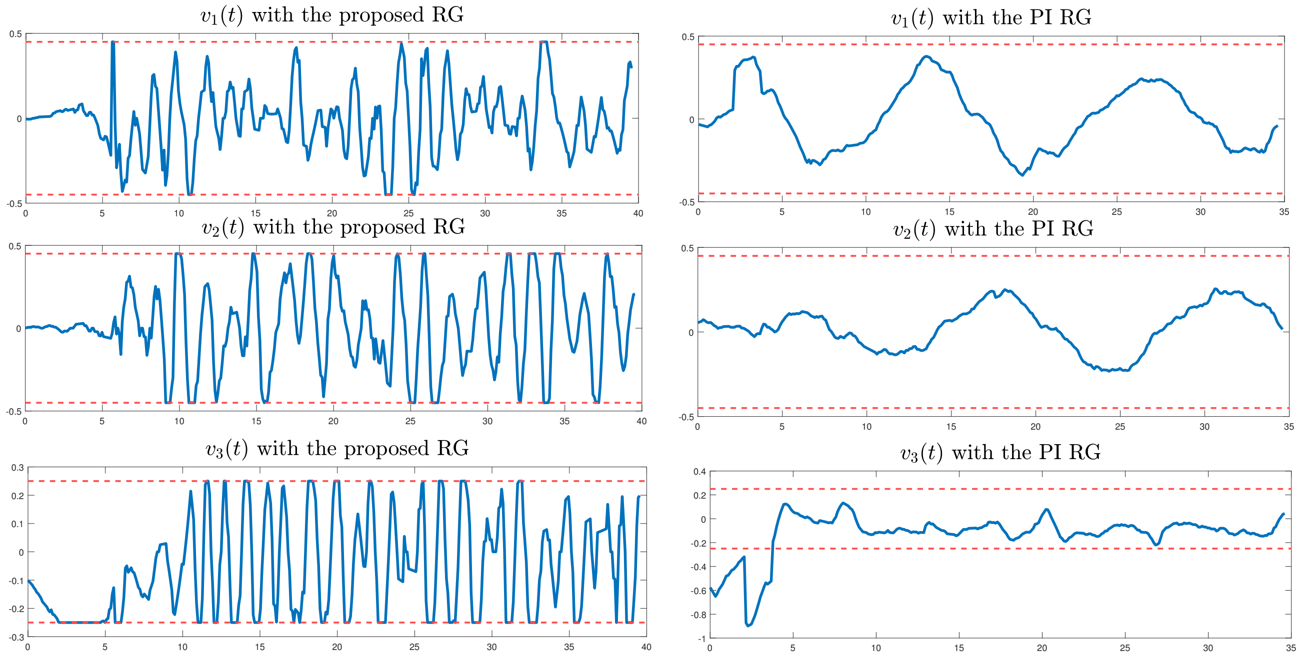

Figure 6. Circular Trajectory: Control command of the proposed (**left**) and PI (**right**) RGs. The blue solid line corresponds to the control signal. The red dashed lines correspond to the saturation levels $\bar{u}_i$ $i = 1, 2, 3$.

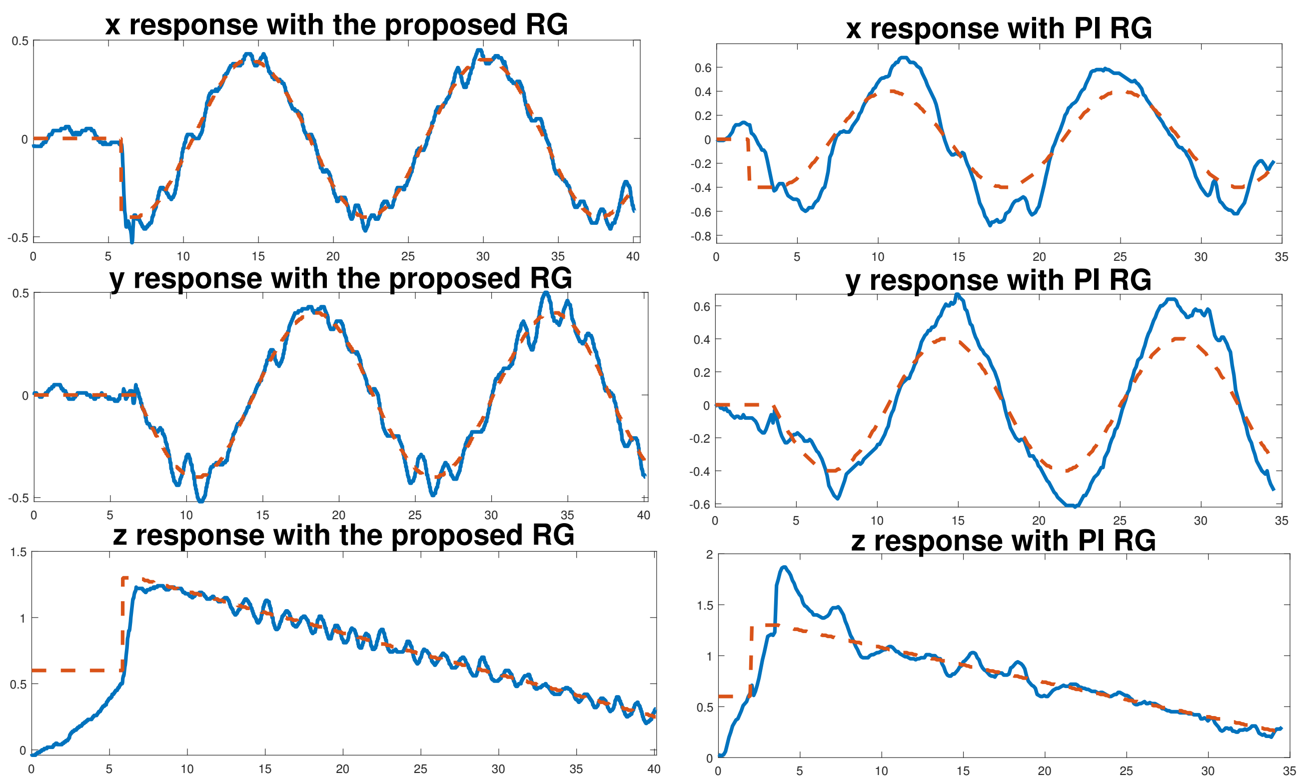

Figure 7. Spiral trajectory: Time response of the quadrotor under the proposed (**left**) and PI (**right**) RGs. The orange dashed line corresponds to the reference trajectory with respect to its principal axis. The blue solid line corresponds to the actual response of the system.

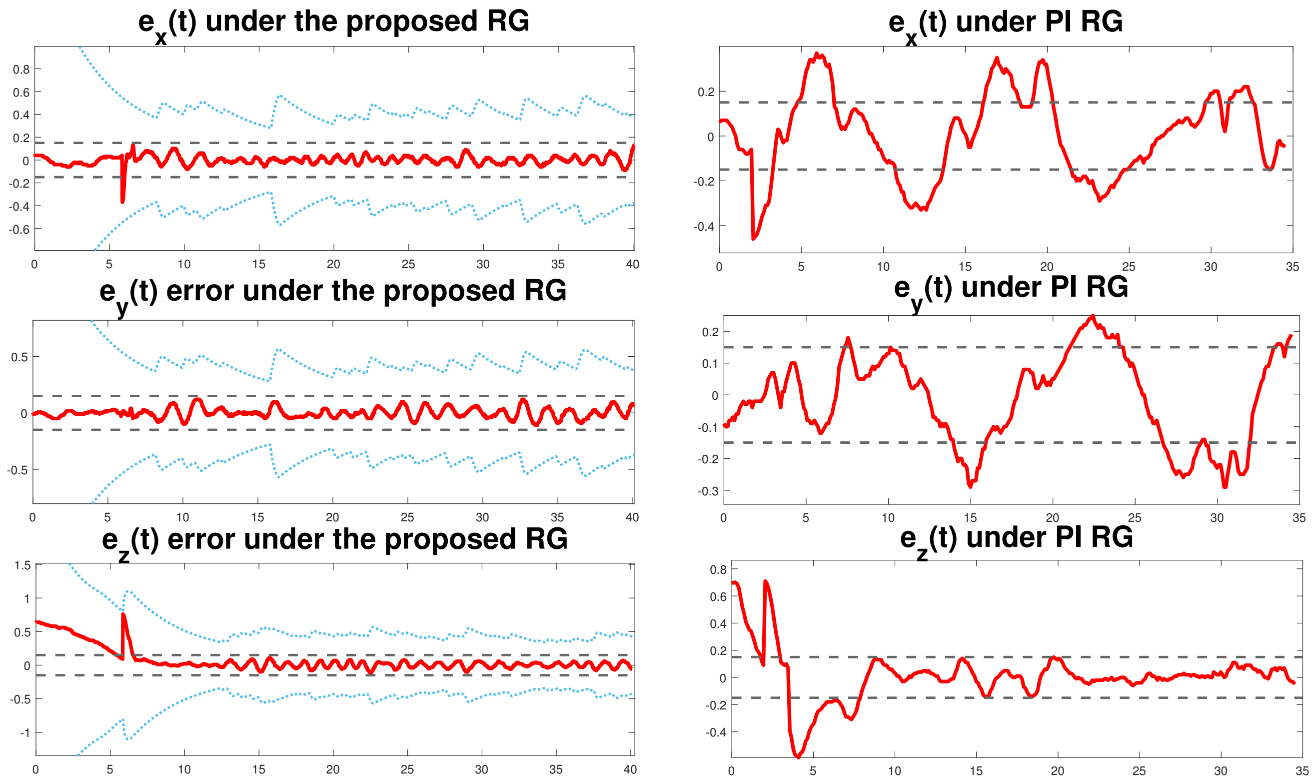

Figure 8. Spiral Trajectory: Output tracking-error evolution of the quadrotor under the proposed (**left**) and PI (**right**) RGs. The light blue dotted lines correspond to the adaptive PFs. The grey dash-dotted lines correspond to the prescribed steady-state error bounds. The red solid line corresponds to the tracking error with respect to its principal axis.

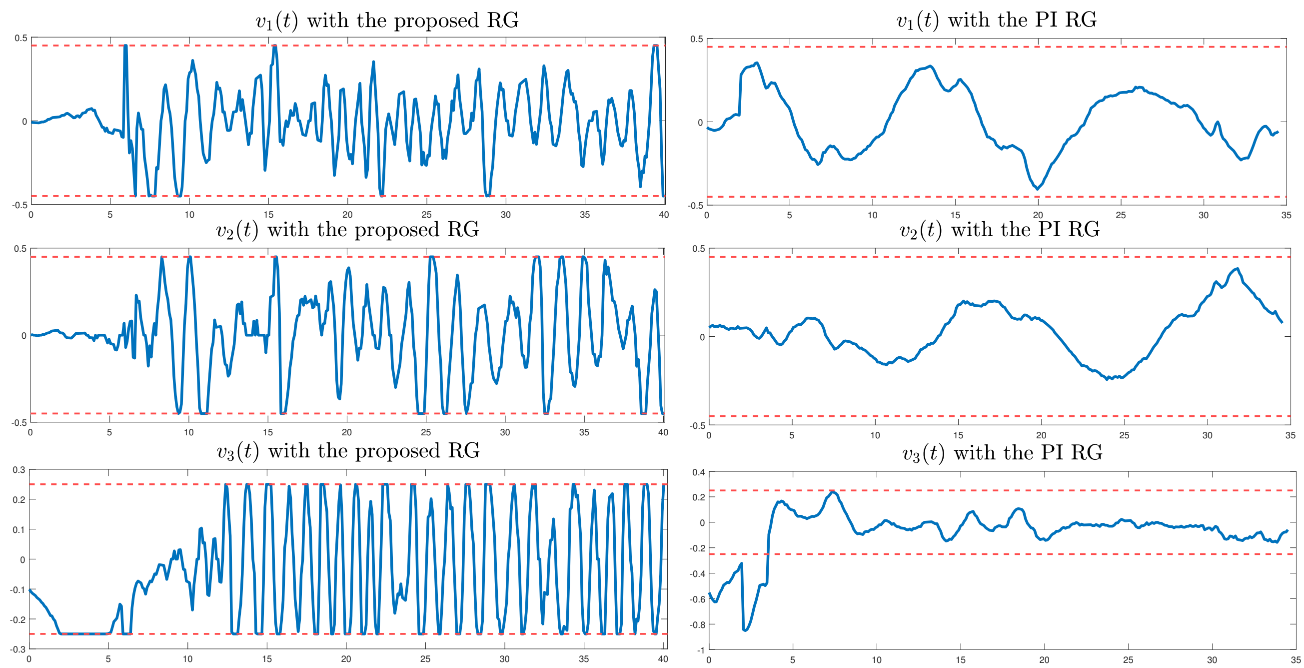

Figure 9. Spiral Trajectory: Control command of the proposed (**left**) and PI (**right**) RGs. The blue solid line corresponds to the control signal. The red dashed lines correspond to the saturation levels $\bar{u}_i$ $i = 1, 2, 3$.

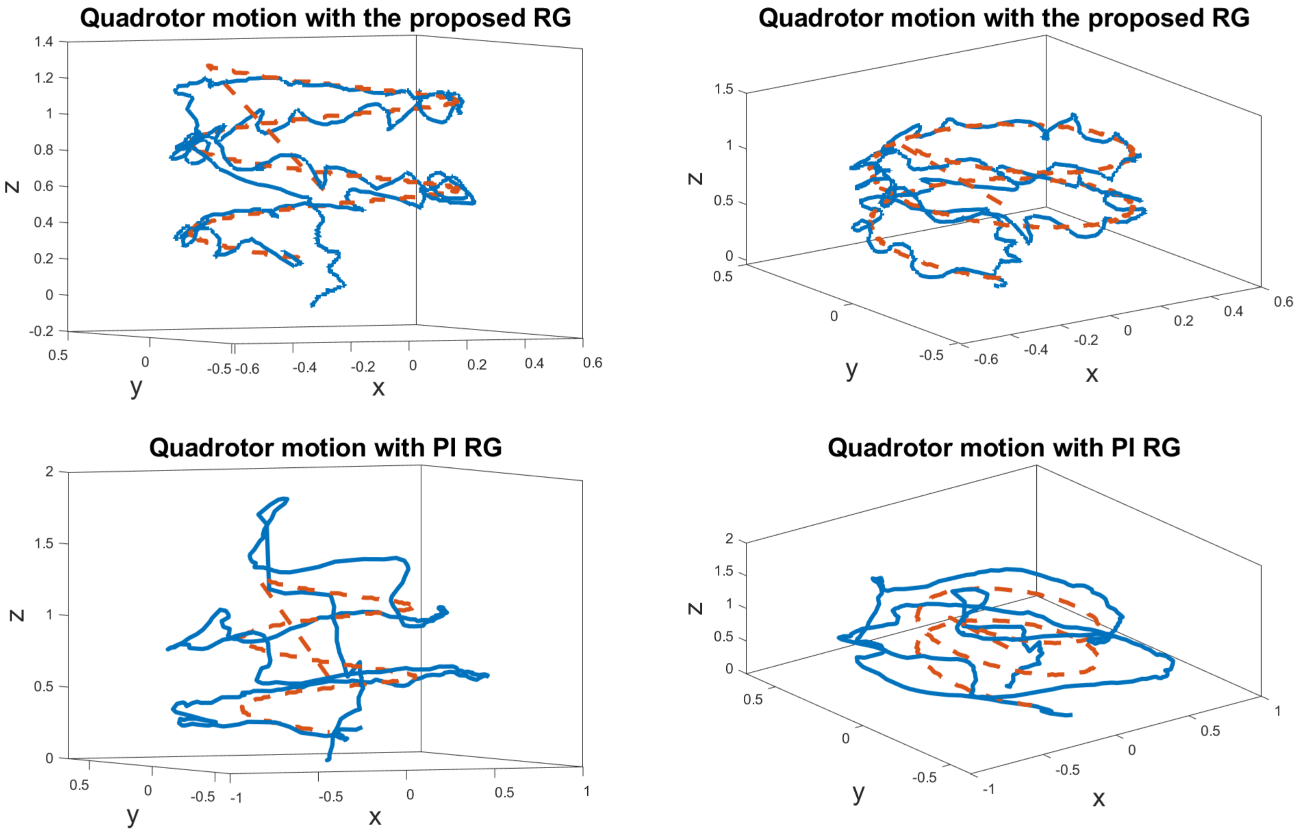

Figure 10. Spiral Trajectory: Three-dimensional motion of the quadrotor under the proposed (**upper** subfigures) and PI (**bottom** subfigures) RGs. The red dashed line corresponds to the reference trajectory. The blue solid line corresponds to the actual response of the system.

4.3. Performance Analysis

The tracking performance of the control schemes is evaluated using four key performance indices, each offering a unique perspective on the system's behavior. In particular, the Average Squared Error index (μ_{ASE}) places greater emphasis on larger errors, indicating a faster convergence rate when its value is lower; the Average Absolute Error index (μ_{AAE}), in contrast to ASE, reflects a slower convergence rate but with reduced persistent oscillations; the Average Time-Weighted Absolute Error index (μ_{ATAE}) focuses on the steady-state error while downplaying initial errors; and finally there is the Total Energy Consumption index (μ_{TEC}), where a lower μ_{TEC} value signifies more efficient energy utilization and reduced energy loss in the control process, quantifying the system's energy efficiency. Furthermore, it should be emphasized in particular that these indices are anticipated to be as small as possible to indicate better control performance and efficiency in the tracking process. For detailed analytical expressions of the performance indices, readers are referred to [38]. In Table 2, we present the aforementioned performance indices as well as the energy of each control input for the two experimental scenarios, allowing a direct and thorough comparison between the proposed RG and the conventional PI controller. Notably, it is essential to highlight that in each case, our method outperforms the PI regulator with respect to the tracking-error metrics, signifying its superior control capabilities. However, the imposition of performance specifications on the system's output demands a more intensive control effort, which consequently leads to higher energy consumption compared to the PI scheme. This is evident from the respective indices presented in Table 2.

Table 2. Tracking Performance Indices.

	Circular Trajectory		Spiral Trajectory	
Performance Index	**Proposed RG**	**PI RG**	**Proposed RG**	**PI RG**
μ_{ASE}	0.043	0.092	0.039	0.093
μ_{AAE}	0.184	0.389	0.163	0.386
μ_{ATAE}	27.771	55.132	23.255	54.698
μ_{TEC}	0.497	0.0.421	0.473	0.395
$\int_0^\infty \lvert v_1(\tau)\rvert^2 d\tau$	1.560	1.160	1.453	1.105
$\int_0^\infty \lvert v_2(\tau)\rvert^2 d\tau$	2.561	0.579	2.171	0.737
$\int_0^\infty \lvert v_3(\tau)\rvert^2 d\tau$	1.345	1.421	1.401	1.364

5. Conclusions

In this work, we proposed a low-complexity robust RG that addresses input constraints for the safe operation of a quadrotor. The exploitation of the adaptive performance control methodology imposes transient and steady-state performance specifications on the output tracking error of the closed-loop system. The straightforward gain selection enables the proposed scheme to be easily integrated in different control tasks without the need of further gain tuning. The theoretical results provide semi-global stability properties for the closed-loop system which are clarified and verified via extensive comparative experimental results between the proposed RG and the well-established PI unit on a commercial quadrotor with limited actuation capabilities.

Regarding future directions, our aim is to extend the proposed RG to multi-robot systems in order to achieve collaborative tasks considering safety constraints to guarantee obstacle and inter-agent collision avoidance as well as communication constraints. Another challenging research direction concerns the development of an adaptive performance control scheme to replace the onboard stabilizing controllers of the quadrotor, further enhancing the performance and the robustness of the closed-loop system.

Author Contributions: Conceptualization, C.P.B.; methodology, P.S.T. and C.P.B.; software, A.T.; validation, P.S.T.; formal analysis, P.S.T.; investigation, P.S.T. and A.T.; writing—original draft preparation, P.S.T.; writing—review and editing, C.P.B.; visualization, P.S.T.; supervision, C.P.B.; project administration, C.P.B. All authors have read and agreed to the published version of the manuscript.

Funding: This work was funded by the Hellenic Foundation for Research and Innovation (H.F.R.I.) under the second call for research projects to support post-doctoral researchers (HFRI-PD19-370).

Institutional Review Board Statement: Not applicable.

Informed Consent Statement: Not applicable.

Data Availability Statement: Not applicable.

Conflicts of Interest: The authors declare no conflict of interest.

Abbreviations

The following abbreviations are used in this manuscript:

APPC	Adaptive Prescribed Performance Control
DOF	Degree Of Freedom
MPC	Model Predictive Control
PF	Performance Function
RF	Reference Governor
UAV	Unmanned Aerial Vehicle

References

1. Masone, C.; Bülthoff, H.H.; Stegagno, P. Cooperative transportation of a payload using quadrotors: A reconfigurable cable-driven parallel robot. In Proceedings of the 2016 IEEE/RSJ International Conference on Intelligent Robots and Systems (IROS), Daejeon, Republic of Korea, 9–14 October 2016; pp. 1623–1630.
2. Naidoo, Y.; Stopforth, R.; Bright, G. Development of an UAV for search & rescue applications. In Proceedings of the IEEE Africon '11, Victoria Falls, Zambia, 13–15 September 2011; pp. 1–6.
3. Shraim, H.; Awada, A.; Youness, R. A survey on quadrotors: Configurations, modeling and identification, control, collision avoidance, fault diagnosis and tolerant control. *IEEE Aerosp. Electron. Syst. Mag.* **2018**, *33*, 14–33. [CrossRef]
4. Yang, L.; Li, B.; Li, W.; Brand, H.; Jiang, B.; Xiao, J. Concrete defects inspection and 3D mapping using CityFlyer quadrotor robot. *IEEE/CAA J. Autom. Sin.* **2020**, *7*, 991–1002. [CrossRef]
5. Gohari, P.S.; Mohammadi, H.; Taghvaei, S. Using chaotic maps for 3D boundary surveillance by quadrotor robot. *Appl. Soft Comput.* **2019**, *76*, 68–77. [CrossRef]
6. Özbek, N.S.; Önkol, M.; Önder Efe, M. Feedback control strategies for quadrotor-type aerial robots: A survey. *Trans. Inst. Meas. Control* **2016**, *38*, 529–554. [CrossRef]
7. Altug, E.; Ostrowski, J.; Mahony, R. Control of a quadrotor helicopter using visual feedback. In Proceedings of the 2002 IEEE International Conference on Robotics and Automation (Cat. No.02CH37292), Washington, DC, USA, 11–15 May 2002; Volume 1, pp. 72–77.
8. Malo Tamayo, A.J.; Villaseñor Ríos, C.A.; Ibarra Zannatha, J.M.; Orozco Soto, S.M. Quadrotor Input-Output Linearization and Cascade Control. *IFAC-PapersOnLine* **2018**, *51*, 437–442. [CrossRef]
9. Lee, D.; Sastry, S. Feedback linearization vs. adaptive sliding mode control for a quadrotor helicopter. *Int. J. Control Autom. Syst.* **2009**, *7*, 419–428. [CrossRef]
10. Fan, Y.; Cao, Y.; Li, T. Adaptive integral backstepping control for trajectory tracking of a quadrotor. In Proceedings of the 2017 4th International Conference on Information, Cybernetics and Computational Social Systems (ICCSS), Dalian, China, 24–26 July 2017; pp. 619–624.
11. Besnard, L.; Shtessel, Y.B.; Landrum, B. Quadrotor vehicle control via sliding mode controller driven by sliding mode disturbance observer. *J. Frankl. Inst.* **2012**, *349*, 658–684. [CrossRef]
12. Ou, T.W.; Liu, Y.C. Adaptive Backstepping Tracking Control for Quadrotor Aerial Robots Subject to Uncertain Dynamics. In Proceedings of the 2019 American Control Conference (ACC), Philadelphia, PA, USA, 10–12 July 2019; pp. 1–6.
13. Iswanto; Wahyunggoro, O.; Cahyadi, A.I. Trajectory and altitude controls for autonomous hover of a quadrotor based on fuzzy algorithm. In Proceedings of the 2016 8th International Conference on Information Technology and Electrical Engineering (ICITEE), Yogyakarta, Indonesia, 5–6 October 2016; pp. 1–6.
14. Emran, B.J.; Najjaran, H. Adaptive neural network control of quadrotor system under the presence of actuator constraints. In Proceedings of the 2017 IEEE International Conference on Systems, Man, and Cybernetics (SMC), Banff, AB, Canada, 5–8 October 2017; pp. 2619–2624.
15. Chen, M.; Xiong, S.; Wu, Q. Tracking Flight Control of Quadrotor Based on Disturbance Observer. *IEEE Trans. Syst. Man Cybern. Syst.* **2021**, *51*, 1414–1423. [CrossRef]
16. Maeder, U.; Borrelli, F.; Morari, M. Linear offset-free Model Predictive Control. *Automatica* **2009**, *45*, 2214–2222. [CrossRef]
17. Mayne, D.; Rawlings, J.; Rao, C.; Scokaert, P. Constrained model predictive control: Stability and optimality. *Automatica* **2000**, *36*, 789–814. [CrossRef]
18. Ngo, K.; Mahony, R.; Jiang, Z.P. Integrator Backstepping using Barrier Functions for Systems with Multiple State Constraints. In Proceedings of the 44th IEEE Conference on Decision and Control, Seville, Spain, 15 December 2005; pp. 8306–8312.
19. Tee, K.P.; Ge, S.S. Control of nonlinear systems with partial state constraints using a barrier Lyapunov function. *Int. J. Control* **2011**, *84*, 2008–2023. [CrossRef]
20. Tee, K.P.; Ge, S.S.; Tay, E.H. Barrier Lyapunov Functions for the control of output-constrained nonlinear systems. *Automatica* **2009**, *45*, 918–927. [CrossRef]
21. Bechlioulis, C.P.; Rovithakis, G.A. Robust Adaptive Control of Feedback Linearizable MIMO Nonlinear Systems With Prescribed Performance. *IEEE Trans. Autom. Control* **2008**, *53*, 2090–2099. [CrossRef]
22. Bechlioulis, C.P.; Rovithakis, G.A. A low-complexity global approximation-free control scheme with prescribed performance for unknown pure feedback systems. *Automatica* **2014**, *50*, 1217–1226. [CrossRef]
23. Berger, T.; Lê, H.H.; Reis, T. Funnel control for nonlinear systems with known strict relative degree. *Automatica* **2018**, *87*, 345–357. [CrossRef]
24. Xu, G.; Xia, Y.; Zhai, D.H.; Cui, B. Adaptive sliding mode disturbance observer–based funnel trajectory tracking control of quadrotor with external disturbances. *IET Control Theory Appl.* **2001**, *15*, 1778–1788. [CrossRef]
25. Zhen, S.; Zhang, L. Unknown System Dynamics Estimator-Based Anti-Disturbance Attitude Funnel Control for Quadrotors with Experimental Verifications. *Electronics* **2022**, *11*, 2136. [CrossRef]
26. Liu, K.; Yang, P.; Wang, R.; Jiao, L.; Li, T.; Zhang, J. Observer-Based Adaptive Fuzzy Finite-Time Attitude Control for Quadrotor UAVs. *IEEE Trans. Aerosp. Electron. Syst.* **2023**, 1–17. [CrossRef]
27. Wang, Y.; Liu, K.; Ji, H. Adaptive robust fault-tolerant control scheme for spacecraft proximity operations under external disturbances and input saturation. *Nonlinear Dyn.* **2022**, *108*, 1–16. [CrossRef]

28. Trakas, P.S.; Bechlioulis, C.P. Robust Trajectory Tracking Control for Constrained Small Fixed-Wing Aerial Vehicles with Adaptive Prescribed Performance. *Appl. Sci.* **2023**, *13*, 7718. [CrossRef]
29. Trakas, P.S.; Bechlioulis, C.P. Robust Adaptive Prescribed Performance Control for Unknown Nonlinear Systems With Input Amplitude and Rate Constraints. *IEEE Control Syst. Lett.* **2023**, *7*, 1801–1806. [CrossRef]
30. Gilbert, E.; Kolmanovsky, I. Nonlinear tracking control in the presence of state and control constraints: A generalized reference governor. *Automatica* **2002**, *38*, 2063–2073. [CrossRef]
31. Bemporad, A. Reference governor for constrained nonlinear systems. *IEEE Trans. Autom. Control* **1998**, *43*, 415–419. [CrossRef]
32. Garone, E.; Di Cairano, S.; Kolmanovsky, I. Reference and command governors for systems with constraints: A survey on theory and applications. *Automatica* **2017**, *75*, 306–328. [CrossRef]
33. Garone, E.; Nicotra, M.M. Explicit Reference Governor for Constrained Nonlinear Systems. *IEEE Trans. Autom. Control* **2016**, *61*, 1379–1384. [CrossRef]
34. Trakas, P.S.; Bechlioulis, C.P. Approximation-free Adaptive Prescribed Performance Control for Unknown SISO Nonlinear Systems with Input Saturation. In Proceedings of the IEEE Conference on Decision and Control, Cancun, Mexico, 6–9 December 2022; pp. 4351–4356.
35. Huang, Z.; Bauer, R.; Pan, Y.J. Closed-Loop Identification and Real-Time Control of a Micro Quadcopter. *IEEE Trans. Ind. Electron.* **2022**, *69*, 2855–2863. [CrossRef]
36. Blösch, M.; Weiss, S.; Scaramuzza, D.; Siegwart, R. Vision based MAV navigation in unknown and unstructured environments. In Proceedings of the 2010 IEEE International Conference on Robotics and Automation, Anchorage, AK, USA, 3–7 May 2010; pp. 21–28.
37. Sontag, E.D. *Mathematical Control Theory: Deterministic Finite Dimensional Systems*, 2nd ed.; Springer: Berlin/Heidelberg, Germany, 1998.
38. Liu, K.; Wang, R.; Wang, X.; Wang, X. Anti-saturation adaptive finite-time neural network based fault-tolerant tracking control for a quadrotor UAV with external disturbances. *Aerosp. Sci. Technol.* **2021**, *115*, 106790. [CrossRef]